

Generalized Brewster Angle Effect in Thin-Film Optical Absorbers and Its Application for Graphene Hydrogen Sensing

Kandammathe Valiyaveedu Sreekanth,^{†,‡,□} Mohamed ElKabbash,^{§,||,□} Rohit Medwal,[⊥] Jihua Zhang,[§] Theodore Letsou,^{||} Giuseppe Strangi,^{||,¶} Michael Hinczewski,^{||} Rajdeep S. Rawat,[⊥] Chunlei Guo,^{*,§,ID} and Ranjan Singh^{*,†,‡,ID}

[†]Division of Physics and Applied Physics, School of Physical and Mathematical Sciences, Nanyang Technological University, 21 Nanyang Link, Singapore 637371

[‡]Centre for Disruptive Photonic Technologies, The Photonic Institute, 50 Nanyang Avenue, Singapore 639798

[§]The Institute of Optics, University of Rochester, 275 Hutchison Road, Rochester, New York 14620, United States

^{||}Department of Physics, Case Western Reserve University, 10600 Euclid Avenue, Cleveland, Ohio 44106, United States

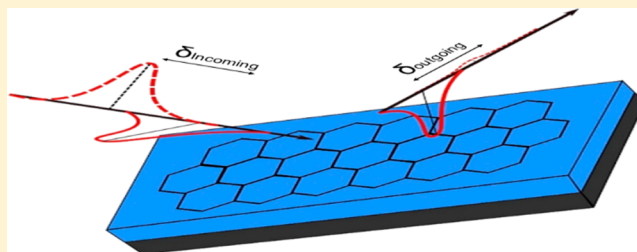
[⊥]Natural Sciences and Science Education, National Institute of Education, Nanyang Technological University, Singapore 637616

[¶]CNR-NANOTEC and Department of Physics, University of Calabria, 87036 Rende, Italy

Supporting Information

ABSTRACT: The generalized Brewster angle (GBA) is the incidence angle at polarization by reflection for p- or s-polarized light. Realizing an s-polarization Brewster effect requires a material with magnetic response, which is challenging at optical frequencies since the magnetic response of materials at these frequencies is extremely weak. Here, we experimentally realize the GBA effect in the visible using a thin-film absorber system consisting of a dielectric film on an absorbing substrate. Polarization by reflection is realized for both p- and s-polarized light at different angles of incidence and multiple wavelengths. We provide a theoretical framework for the generalized Brewster effect in thin-film light absorbers. We demonstrate hydrogen gas sensing using a single-layer graphene film transferred on a thin-film absorber at the GBA with ~ 1 fg/mm² aerial mass sensitivity. The ultrahigh sensitivity stems from the strong phase sensitivity near the point of darkness, particularly at the GBA, and the strong light–matter interaction in planar nanocavities. These findings depart from the traditional domain of thin films as mere interference optical coatings and highlight its many potential applications including gas sensing and biosensing.

KEYWORDS: Brewster angle effect, thin-film optics, perfect absorbers, visible frequencies, graphene, gas sensing



The Brewster angle, θ_B , is commonly defined as the angle at which the Fresnel's reflection coefficients for p-polarized light vanishes.¹ For a given medium, the sum of the incident angle θ_i and transmitted angle θ_t is $\pi/2$ when $\theta_i = \theta_B$. The orthogonality condition draws a simple picture for realizing the Brewster angle effect. Light incident on a medium at θ_B induces electron oscillations in the direction of the electric field, which give rise to reflected wavelets. The oscillating electrons, however, do not produce a field at points on the axis of oscillation. When $\theta_i + \theta_t = \pi/2$, the oscillation axis is in the direction of the reflected wave; hence, no reflection takes place. The Brewster effect is widely used in different applications, e.g., reducing glare of sun reflecting off horizontal surfaces and in laser physics in gain media, cavity mirrors, and in prisms to minimize reflection losses, as well as in high-performance terahertz modulators.² Furthermore, Brewster angle microscopes rely on the enhanced phase sensitivity near the Brewster angle and can image monolayers

at the air–liquid interface.^{3,4} However, the phase sensitivity at the Brewster angle is thought to be insufficient for sensing applications, as the local electric fields for dielectric substrates are small.⁴

The aforementioned common definition of the Brewster angle, however, assumes that the reflection occurs from a plane wave incident on a homogeneous, nonmagnetic, achiral, and isotropic material. The Brewster effect can take place for either p- or s-polarized light if one of these assumptions is violated. For example, it is known that a Brewster angle for s-polarized light exists in a magnetic material with permeability $\mu \neq 1$. In magnetic materials, there exists an angle where the reflected s-polarized light vanishes, θ_B^s , and another angle where the reflected p-polarized light vanishes, θ_B^p , such that $\theta_B^s \neq \theta_B^p$ for non-normal incidence.⁵ For a magnetic medium, the sum of

Received: April 14, 2019

Published: June 18, 2019

the incident angle and the generalized Brewster angles (GBAs) $\theta_B^{p,s}$ does not need to be $\pi/2$ as long as total destructive interference between the magnetic and electric dipoles takes place at $\theta_B^{p,s}$. Accordingly, the Brewster effect can take place even when the oscillation axis is not parallel to the wave reflection direction and the wavelets produced by individual oscillating electrons do not vanish at the reflection direction. What is necessary, however, is that the vector sum of the radiated field vanishes in the reflection due to destructive interference.⁶ The Brewster angle, in its most general form, is the angle where *only* a single polarization is reflected due to the destructive interference between radiating electric and/or magnetic dipoles for the orthogonal polarization.

Realizing a generalized Brewster effect at optical frequencies is challenging since the magnetic response of materials at these frequencies is very weak, i.e., $\mu \approx 1$. Metamaterials, however, can support negative permeability; thus a magnetic response is possible.^{7–9} The generalized Brewster effect was realized experimentally using split ring resonators in the microwave region.^{10,11} In the optical regime, a GBA effect was demonstrated using all-dielectric metamaterials.¹² In addition to the intense lithography required to fabricate a metamaterial with a magnetic response, the Brewster angle demonstrated did not realize complete polarization of the reflected light in the visible frequencies, particularly for s-polarized light.¹² Strictly speaking, however, this demonstration did not exhibit a true Brewster effect, but rather showed unequal reflection for s- and p-polarizations, which is a natural consequence of the Fresnel equations even in the absence of any magnetic response. On the other hand, an s-polarized Brewster effect was shown in stratified metal–dielectric metamaterials due to changes in the effective magnetic permeability of the thin-film stack.¹³ In addition, for nonmagnetic media, the s-polarized Brewster effect was demonstrated by adding a two-dimensional material at the interface between two media when the conditions for total internal reflection are satisfied such that reflected s-polarized light is absorbed fully by the graphene layer.¹⁴ Furthermore, GBA was demonstrated in anisotropic materials¹⁵ and chiral materials.¹⁶

The assumption that the reflection occurs from a homogeneous medium can also be violated by creating a multilayer structure where either the s- or the p-polarized light is reflected and the other polarization is extinguished.¹⁷ The generalized Brewster conditions of a lithography-free planar stack of thin films have been theoretically investigated where the inhomogeneity is due to stacking different materials.^{18–24} In this case, the GBA corresponds to an angle where electric dipoles in the inhomogeneous stack of materials destructively interfere. An experimental realization of GBA effect of a transparent film on an absorbing substrate, however, has not been demonstrated. Furthermore, the realization of the generalized Brewster effect can be used for sensing applications providing that it is associated with strong field localization.

In this Letter, we investigate theoretically and experimentally the generalized (p- and s-polarization) Brewster conditions of a lossless dielectric film on an absorptive substrate at multiple wavelengths in the visible spectral region. By demonstrating, thin-film interference based perfect light absorption of a single polarization, the Brewster effect, i.e., polarization by reflection, is realized for both s- and p-polarized light at different angles of incidence. We further demonstrate hydrogen sensing using a hybrid platform of single-layer graphene and the thin-film absorber. The realization of phase singularity in the

ellipsometry phase parameter at the GBA accompanied by strong field confinement within the graphene layer in the thin-film cavity enabled ultrahigh hydrogen sensitivities of ~ 1 fg/mm² with cheap materials and a scalable fabrication process.

■ THEORY OF GENERALIZED BREWSTER EFFECT IN THIN-FILM LIGHT ABSORBERS

We investigate the proposed design, i.e., a lossless dielectric film on a substrate with optical losses. Our system consists of a superstrate (refractive index n_0), a dielectric layer (refractive index n_d , thickness d), and a lossy substrate (refractive index $n_s + ik_s$). Using transfer matrix theory,²⁵ we obtain expressions for the conditions necessary to realize the GBA effect for p- and s-polarized light in terms of the incidence angle (θ_0) and the phase thickness of the dielectric layer, $\Phi_d \equiv 2\pi d\lambda^{-1} \sqrt{n_d^2 - n_0^2 \sin^2(\theta_0)}$ (see Supporting Information for detailed derivation).

i. p-Polarization.

$$\theta_0 \approx \tan^{-1} \left[\frac{n_s}{n_0} \left(1 + \frac{1}{2} k_s^2 \left(\frac{n_0^2 (n_0^2 - 3n_d^2)}{(n_0^2 - n_d^2) n_s^4} + \frac{2(n_0^2 (2n_d^2 - 3n_s^2) + n_s^4)}{n_s^2 (n_s^2 - n_0^2) (n_s^2 - n_d^2)} \right) \right) \right]$$

$$\tan(\Phi_d) \approx \frac{n_d^2 k_s (n_s^2 - n_0^2) \sqrt{n_0^2 (n_d^2 - n_s^2) + n_d^2 n_s^2}}{(n_0^2 - n_d^2) n_s^3 (n_s^2 - n_d^2)} \quad (1)$$

The first condition above defines a unique GBA θ_0 at which the p-polarized reflection is zero. Note that when $k_s \rightarrow 0$, it reduces to the standard Brewster angle, $\theta_0 \rightarrow \tan^{-1}(n_s/n_0)$. For finite k_s with the materials we use, the correction due to a lossy substrate is quite small, so θ_0 remains close to the conventional Brewster angle. The $\tan(\Phi_d)$ condition can be solved to find a set of dielectric layer thicknesses d that will give zero reflection (there is more than one possibility since $\tan(\Phi_d + m\pi) = \tan(\Phi_d)$ for any integer m). Note that when $k_s \rightarrow 0$, this condition reduces to $\tan(\Phi_d) = 0$. In this case, one possible solution is $d = 0$, the conventional case where no dielectric layer is present. In addition, the conventional Brewster effect ($\theta_0 = \tan^{-1}(n_s/n_0)$) is realized for other d values that satisfy $\tan(\Phi_d) = 0$. However, when $k_s > 0$, we need a finite $d > 0$ to achieve zero reflection; that is, there is no Brewster angle for a dielectric with optical losses unless we add an additional lossless dielectric with finite thickness.

ii. s-Polarization. To get zero reflection for s-polarization, the real parts of the refractive indices must satisfy $n_0 n_s > n_d$. Additionally, to get compact expressions, we assume $n_s > n_d > n_0$. The conditions are then given by

$$\theta_0 \approx \tan^{-1} \left[\sqrt{\frac{n_0^2 n_s^2 - n_d^4}{(n_0^2 - n_d^2)^2}} \left(1 + k_s^2 \frac{n_0^2 (n_d^4 - (n_0^2 - 2n_d^2) n_s^2 - 2n_s^4)}{2(n_d^2 - n_s^2)^2 (n_d^4 - n_0^2 n_s^2)} \right) \right]$$

$$\tan(\Phi_d) \approx \frac{(n_d^2 - n_s^2)^2}{n_s k_s \sqrt{(n_0^2 - n_d^2) (n_d^2 - n_s^2)}} \quad (2)$$

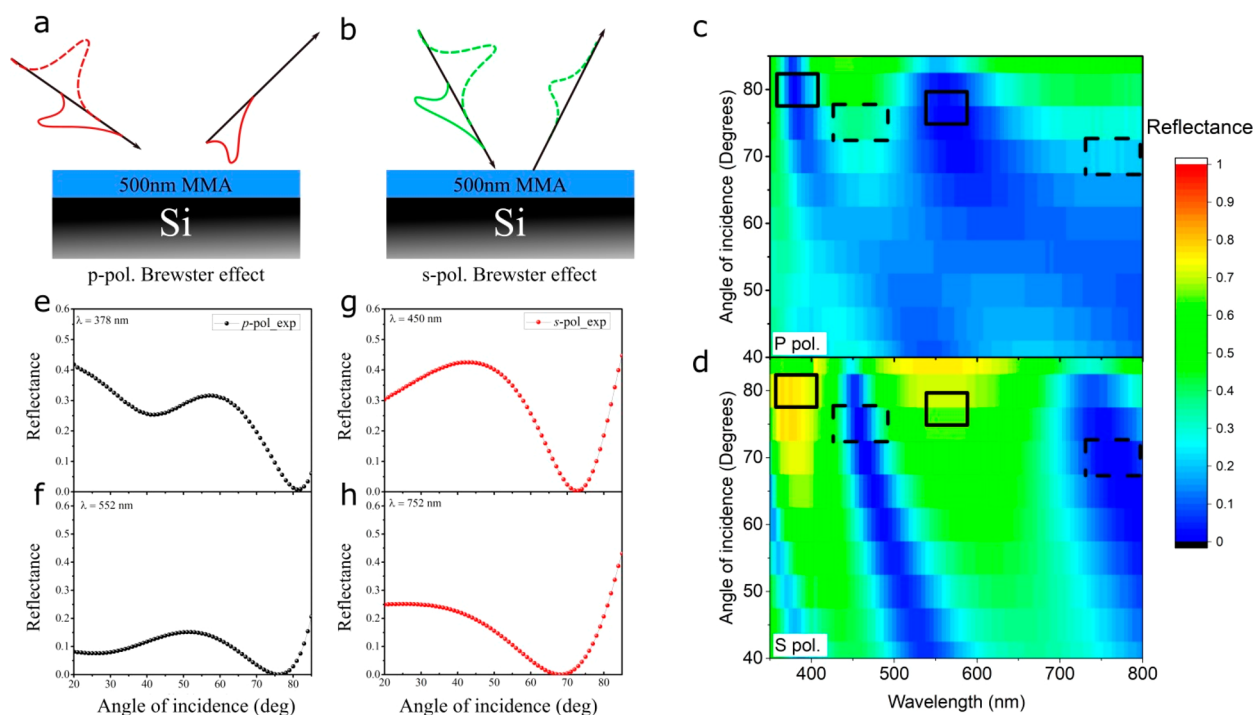


Figure 1. Generalized Brewster effect in a thin-film dielectric on a lossy substrate system. Schematic of the MMA (500 nm)–Si light absorber exhibiting (a) p-polarized Brewster effect and (b) s-polarized Brewster effect. Measured angular reflectivity spectra for a (c) p-polarized and (d) s-polarized reflectance spectrum of the thin-film absorber. The rectangulated regions refer to wavelength and angle pairs where the generalized Brewster effect occurs for p-polarized light (solid squares) and s-polarized light (dashed squares). Measured angular reflectance is shown for p-polarization at (e) 378 nm and (f) 552 nm and for s-polarization at (g) 450 nm and (h) 752 nm.

As with s-polarization, the presence of k_s makes only minor corrections to the angle and thickness results. In the limit $k_s \rightarrow 0$ we find $\theta_0 \rightarrow \tan^{-1} \sqrt{(n_0^2 n_s^2 - n_d^2) / (n_0^2 - n_d^2)^2}$ and $\tan(\Phi_d) \rightarrow \infty$. The latter implies that Φ_d in the lossless case must be equal to $(2m + 1)\pi/2$ for $m = 0, 1, 2, \dots$. Now $d = 0$ is no longer a valid solution, so one needs a dielectric layer to get zero reflection even when $k_s = 0$. When $k_s > 0$, the value of Φ_d is shifted slightly away from these odd multiples of $\pi/2$, and hence $\tan(\Phi_d) < \infty$.

EXPERIMENTAL VERIFICATION USING METHYL METHACRYLATE COATED SILICON SUBSTRATE

To experimentally show that a transparent dielectric film on an absorbing substrate exhibits a GBA effect in the visible, we spin coated a methyl methacrylate (MMA) layer with thickness $t = 500$ nm on a silicon (Si) substrate, which demonstrates a p-polarized Brewster effect (Figure 1a) and s-polarized Brewster effect (Figure 1b) at different wavelengths and angles of incidence. We measured the reflectance spectra as a function of wavelength (350 to 800 nm) and angle of incidence (40° to 85°) using a spectroscopic ellipsometer; see the Supporting Information. The false-color 2D plot of measured reflectance spectra of p- and s-polarization is shown in Figure 1c and d, respectively. In particular, p-polarization exhibits low reflection above an incidence angle of 60° , and all angle minimum reflection is obtained for s-polarization. However, zero reflection is only possible for a single wavelength and at the Brewster angle for both polarizations. Accordingly, the thin-film absorber supports GBA for multiple wavelengths (Supporting Information Figure S2). The rectangulated regions refer to wavelength and angle pairs where the generalized Brewster effect occurs for p-polarized light (solid

squares) and s-polarized light (dashed squares). Clearly, the thin-film absorber supports two modes in the wavelength range of interest for both p- and s-polarizations.

To further clarify the generalized Brewster effect, we performed reflectance measurements as a function of incidence angle by selecting the wavelength in which zero reflection is obtained for both polarizations. We note that since the substrates used in experiments are opaque, absorptance (A) is complementary to reflectance (R), i.e., $A = 1 - R$. Accordingly, when $R \rightarrow 0$, the structure exhibits perfect light absorption. For p-polarization, zero reflection is obtained at 378 and 552 nm, as shown in Figure 1e and f, respectively. The recorded Brewster angle for p-polarization at 378 and 552 nm is 81° and 76° , respectively. For s-polarization, zero reflection is obtained at 450 and 752 nm, as shown in Figure 1g and h, respectively. The obtained Brewster angle for s-polarization at 450 and 752 nm is 73° and 68° , respectively. The calculated p- and s-polarization angular reflection was obtained using the transfer matrix method (Supporting Information Figure S3). In the model, we solved the Fresnel equations for a three-layer system (air–MMA (500 nm)–Si), and experimentally obtained refractive indices of MMA were used.^{26,27} It is important to note that the Brewster angle increases with decreasing the incident wavelength for both polarizations in order to satisfy the amplitude condition for total destructive interference; that is, the amplitude of the out-of-phase partially reflected waves from all interfaces must be equal in magnitude.²⁸ This is because at lower wavelengths the reflectance from Si is significantly high. Accordingly, to satisfy the amplitude condition, the reflection from MMA must increase, which is only possible at high incidence angles. We simulated the field distribution of the MMA/Si system at the Brewster angles

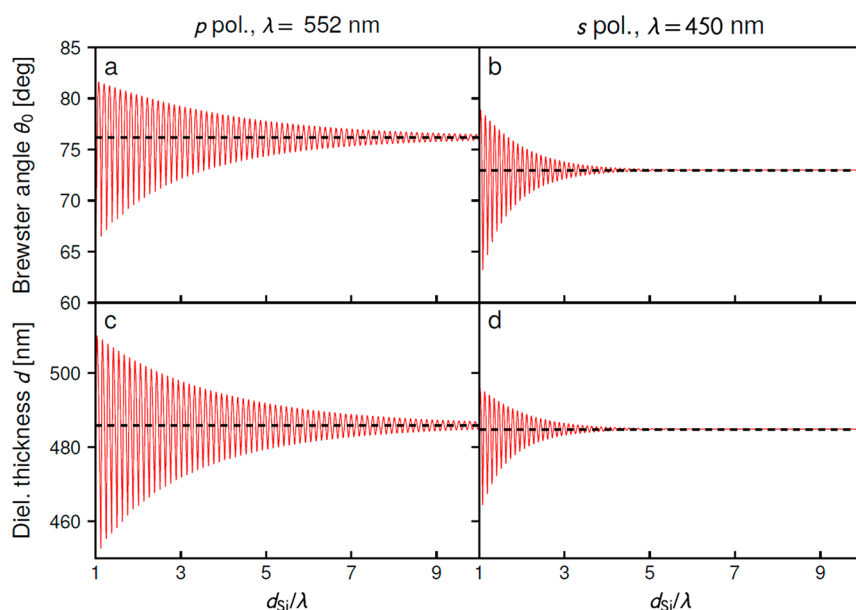


Figure 2. Numerical transfer matrix theory results showing the conditions needed to achieve the generalized Brewster angle effect when the lossy substrate layer has a finite thickness. The system consists of an MMA layer of thickness d and a Si layer of thickness d_{Si} on glass. The top row shows the incidence angle needed to realize the Brewster effect as a function of d_{Si}/λ for (a) p-polarization, incident wavelength $\lambda = 552$ nm; (b) s-polarization, incident wavelength $\lambda = 450$ nm. The bottom row (c, d) shows the corresponding MMA layer thickness d that is required as an additional condition. The dashed lines correspond to the theoretical predictions for an infinite Si layer, described in eqs 1 and 2.

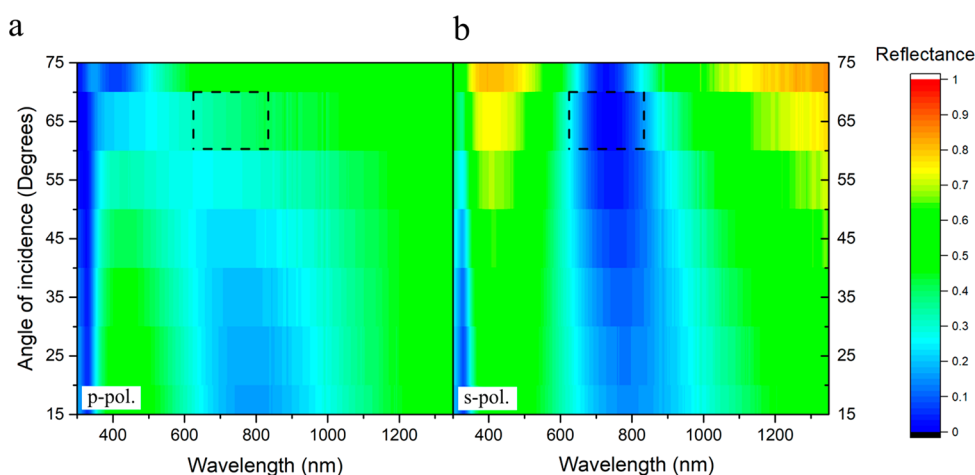


Figure 3. Generalized Brewster angle effect (s-polarized) using a light-absorbing thin-film metasurface. Angular reflectivity spectra. Measured (a) p-polarized and (b) s-polarized reflectance spectrum.

(Supporting Information Figure S4). We have also experimentally investigated the GBA effect in an MMA–Ge–glass system and confirmed that this system shows similar Brewster angles; however the incident wavelengths where the effect is observed are slightly red-shifted (Supporting Information Figure S5 and Figure S6).

Note that the system still exhibits the GBA effect even when the lossy substrate is a layer of finite thickness. The mathematical conditions for zero reflectance no longer have tractable analytical forms, but the infinite substrate theory in eqs 1 and 2 remains a reasonable approximation even when the lossy layer thickness is comparable to the wavelength of the incident light. We can see this in Figure 2, which shows incidence angle (top row) and dielectric layer thickness d (bottom row) needed to ensure zero reflectance for each polarization. The oscillation in GBA as a function of thickness is due to additional Fabry–Perot interference effects due to the

finite thickness of Si. Figure 2 was calculated for an MMA layer of thickness d on top of a Si layer of thickness d_{Si} on top of glass and is plotted as a function of d_{Si}/λ , where λ is the incident wavelength. The dashed lines represent the predictions of the theory for infinite Si. One can see that as d_{Si} gets larger, the results converge to the theory predictions. The deviations increase as d_{Si} approaches λ , but within this range are still typically less than 10%.

■ EXPERIMENTAL VERIFICATION USING LIGHT-ABSORBING THIN-FILM METASURFACE

Perfect light absorption can occur in ultrathin dielectrics with $t \ll \lambda$; that is, the dielectric coating does not need to satisfy the antireflection coating condition of $t = (\lambda/4)n$. This takes place in a two-layer system with a dielectric coating and a substrate, when the destructive interference phase condition is satisfied

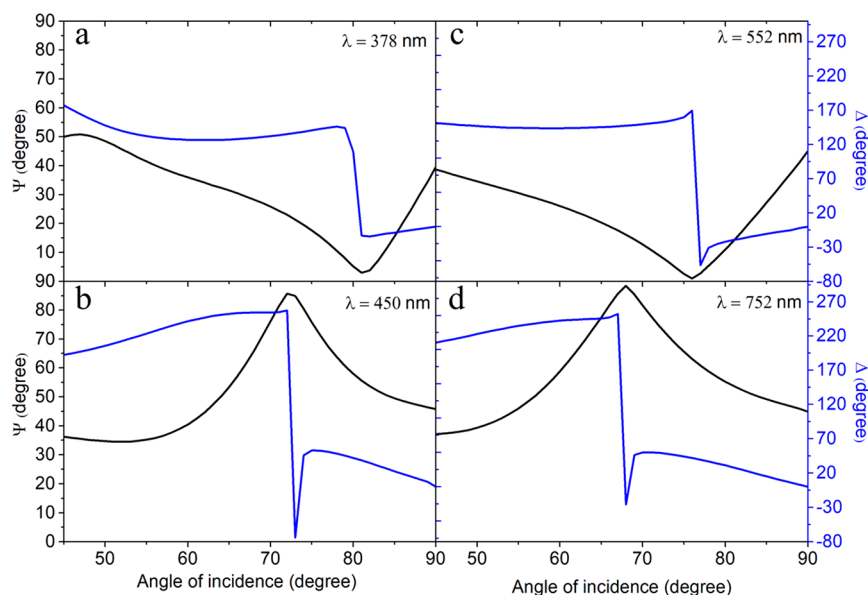


Figure 4. Measured pair of ellipsometry parameters (ψ and Δ) (a) at 378 nm, (b) at 450 nm, (c) at 552 nm, and (d) at 752 nm. A singular phase is obtained at GBAs in which ψ is minimum/maximum values.

due to the existence of an abrupt phase change; that is, the phase is either 0 or π , at the air/dielectric or the dielectric/substrate interfaces.²⁹ Because the perfect light absorption in ultrathin films relies on acquiring a phase and not propagating in a refractive medium, these thin-film light absorbers are considered metasurfaces.³⁰

Figure 3 shows the angular reflectance spectrum for an ultrathin perfect light absorber consisting of a 60 nm TiO₂ film on a 100 nm Ni substrate. For p-polarized light, perfect light absorption does not occur at any angle or wavelength (Figure 3a). On the other hand, the Brewster angle occurs at 750 nm and 68° for s-polarized light (Figure 3b). The refractive index of TiO₂ at 750 nm is ~ 2.5 , i.e., $t = (\lambda/5)n$.

■ EXPERIMENTAL VERIFICATION OF SINGULAR PHASE AT THE GBAS

Ellipsometry measures the complex reflectance of a system, ρ , which is parametrized by the amplitude component Ψ and the phase difference Δ , such that $\tan \Psi = \frac{|r_p|}{|r_s|}$ and $\Delta = \delta_{\text{outgoing}} - \delta_{\text{incoming}}$, where δ is the phase difference between the p-polarized and s-polarized light, such that $\rho = \frac{r_p}{r_s} = \tan \Psi e^{i\Delta}$. Accordingly, ellipsometry parameters (Ψ , Δ) have unique characteristics at the Brewster angle. In particular, Ψ reaches a minimum (maximum) at the Brewster angle for p-polarized (s-polarized) light. Furthermore, beyond the Brewster angle, the reflection phase undergoes a $\sim \pi$ phase shift. Accordingly, we can obtain a singular phase (phase difference between p- and s-polarization) of the reflected light at the zero-reflection wavelength and angle. We show that the lossless dielectric-absorbing substrate system provides a singular phase at the Brewster angles of both p- and s-polarizations.

We experimentally measure the ellipsometry parameters Ψ and Δ using a variable-angle high-resolution spectroscopic ellipsometer. The experimentally obtained Ψ and Δ spectra of a transparent film-absorbing substrate system for wavelengths 378, 450, 552, and 752 nm are shown in Figure 4a, b, c, and d, respectively. Note that ψ can vary from 0 to 90° and Δ ranges

from 0 to 360° (or -180° to $+180^\circ$). It is clear that minimum/maximum Ψ values and singular Δ phases are obtained at the GBAs. For 378 and 552 nm wavelengths (Figure 4a and c), a minimum Ψ corresponds to the Brewster angle for p-polarized light. On the other hand, a maximum Ψ is obtained at 450 and 752 nm (Figure 4b and d), corresponding to the Brewster angle for s-polarized light.

■ HYDROGEN SENSING WITH SINGLE-LAYER GRAPHENE TRANSFERRED ON THIN-FILM OPTICAL ABSORBERS

At ambient pressure and temperature, hydrogen is colorless, tasteless, and highly flammable.³¹ Hydrogen is flammable at concentrations ranging from 4% to 75% with low ignition energy. Accordingly, hydrogen sensing is largely used in industries where it is a necessary component or a byproduct to monitor and control the hydrogen partial pressure for safety purposes. Hydrogen is also produced by certain bacteria, and hydrogen sensors are used in the food industry and have possible medical applications.^{32–35} Furthermore, hydrogen sensing is important for fuel cell applications to investigate the loading or unloading kinetics of hydrogen in nanostructured materials.

Various electrical hydrogen sensors based on semiconductors, protonic conductors, and platinum wires have been proposed.³¹ However, these systems show enhanced sensitivity only at higher temperatures, which is a major safety issue. In contrast to electrical detection of hydrogen, optical detection techniques offer higher sensitivity in ambient environments, fast response times, and low power consumption. Furthermore, elimination of electric currents and possible sparks in hydrogen-rich environments minimizes the risk of explosion. Many approaches for optical hydrogen sensing have been demonstrated using palladium-based optical systems.^{36–42} However, most of the palladium-based optical hydrogen sensors reported to date rely on intense lithography techniques.

Here, we exploit the singular phase behavior^{4,26} of our devices at the GBA to detect changes in the optical properties

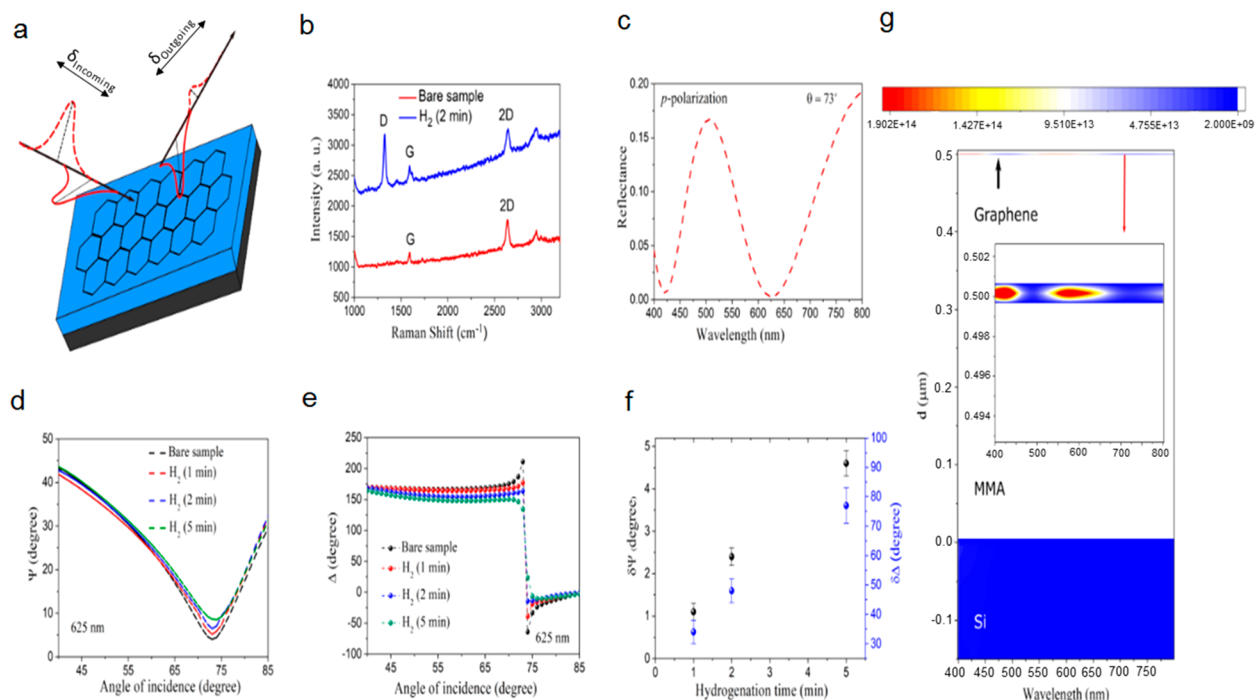


Figure 5. Experimental demonstration of hydrogen sensing using the graphene–MMA–Si system. (a) Schematic of the fabricated graphene–MMA–Si system. (b) Raman spectrum of bare graphene and hydrogenated graphene acquired from the fabricated structure. The excitation wavelength was 633 nm. (c) Measured p-polarized reflectance spectrum of the graphene–MMA–Si system at 73°. The measured (d) ψ and (e) Δ spectrum of graphene–MMA–Si and hydrogenated graphene–MMA–Si for different times at 625 nm. The maximum ψ and Δ change is obtained at the Brewster angle. (f) Marginal ψ and Δ shifts with different hydrogenation times. (g) FDTD calculation of the power dissipation density inside the graphene–MMA–Si structure at normal incidence showing an order of magnitude higher power dissipation in the graphene layer.

of the thin-film device for hydrogen sensing. Accordingly, we use a transferred graphene layer on the lossless dielectric–lossy substrate light absorber to detect low hydrogen concentrations. The device functions as a lithography-free, large-area, and inexpensive hydrogen sensor. Graphene is particularly attractive, as it can reversibly react with atomic hydrogen.^{43,44} Upon hydrogenation, graphene changes its optical properties as it transitions from a semimetal to an insulator.⁴³ Furthermore, it was shown that the light–matter interaction of ultrathin films can enhance drastically based on a strong interference effect in thin-film light absorbers which overcome the limitation between the optical absorption and film thickness.⁴⁵ The strong field confinement inside the graphene layer results in ultrahigh sensitivity to the graphene optical properties, which we exploit for high-sensitivity hydrogen sensing.

Figure 5a is a schematic of the device showing the incoming and outgoing beams undergoing polarization-dependent change in amplitude and phase. A CVD-grown single-layer graphene was transferred on an MMA–Si system using the conventional graphene transfer process. The red curve in Figure 5b shows the Raman spectrum of graphene measured on the fabricated sample. The relative intensity of G and 2D peaks confirms that the transferred graphene is a single layer. The experimentally obtained p-polarized reflectance spectrum at 73° incidence angle is shown in Figure 5c. Adding a single-layer graphene red-shifts the absorption modes; however, perfect light absorption is exclusively realized for p-polarized light at 625 nm wavelength and 73° angle of incidence. The red shift in the absorption modes is due to the high complex refractive index of graphene in the visible spectrum⁴⁶ (Supporting Information Figures S8 and S9). The addition

of graphene further modifies the reflection phase and ellipsometry parameters of the entire system (Supporting Information Figures S10 and S11). The sensitivity of the mode location on the graphene layer implies that graphene surface chemistry can be effectively studied using the Brewster angle concept. We consider this mode to demonstrate phase-sensitive hydrogen sensing as described below.

The measured ellipsometry parameters ψ and Δ of the graphene–MMA–Si system at 625 nm are shown as a black curve in Figure 5d and e, respectively. One can see that singular phase is obtained at the Brewster angle (73°), where the ψ value is a minimum. To demonstrate ultrahigh sensitivity of the thin-film optical absorber for hydrogen sensing, we used a plasma hydrogenation procedure. In particular, a graphene–MMA–Si sample was exposed to different concentrations of atomic hydrogen by controlling the hydrogenation time. As a first step, we studied the Raman spectral features using hydrogenated samples. The hydrogenated graphene shows an additional sharp Raman D peak at about 1340 cm^{-1} , which is activated by defects.^{43,44} In Figure 5b, we show the emergence of a Raman D peak around 1340 cm^{-1} after hydrogenation of the sample (blue curve), which shows the chemical reaction of atomic hydrogen with graphene (Supporting Information Figure S12). On the other hand, the D peak does not exist for graphene with no hydrogenation.

The measured ψ and Δ spectra of the sample with different hydrogenation times (1–5 min) are shown in Figure 5d and e. The marginal ψ and Δ shifts at the Brewster angle (73°) with respect to unhydrogenated graphene–MMA–Si sample are shown in Figure 5f. The variation in ψ and Δ increased with increasing hydrogenation time. However, a drastic change in Δ is obtained at the Brewster angle compared to the ψ change. By

considering the phase change obtained for 1 min hydrogenation time (34°) and phase resolution of the instrument ($<1^\circ$), an areal mass sensitivity on the order of $1 \text{ fg}/\text{mm}^2$ can be achieved using the proposed platform. To put this in context, a GBA graphene gas sensor provides $\delta\psi = 1^\circ$ and $\delta\Delta = 34^\circ$ after 1 min of hydrogen exposure and $\delta\psi = 4.5^\circ$ and $\delta\Delta = 75^\circ$ after 5 min of hydrogen exposure as compared to the singular-phase plasmonic–graphene hydrogen sensor, which provided $\delta\psi = 2^\circ$ and $\delta\Delta = 50^\circ$ after 20 min of hydrogen exposure.⁴ Furthermore, we calculated the power dissipation density (W/m^2) in the graphene–MMA–Si structure using the finite difference time domain (FDTD) method. Figure 5g shows the calculated power dissipation density (W/m^2) in the graphene–MMA–Si structure as a function of wavelength at normal incidence (also see Supporting Information Figure S13). Surprisingly, the power dissipation density is an order of magnitude higher inside the graphene layer compared to the Si substrate. Enhanced light absorption in graphene was previously shown in the UV range using coherent light absorption in the multilayer thin-film structure⁴⁷ and in the visible and NIR wavelength ranges using a grating consisting of a multilayer graphene–dielectric stack.⁴⁸ Accordingly, the obtained ultrahigh sensitivity is due to the strong phase sensitivity at the Brewster angle and the strong light–matter interaction at the graphene film. We note here that upon extended hydrogenation, graphene absorption is quenched in the UV, visible, and IR frequencies.⁴⁹

Since the sample required annealing above 200°C for reversible hydrogenation,^{43,44} the demonstration of reversible hydrogenation is not possible using the MMA-based thin-film optical absorbers. Nevertheless, the proposed platform can be used to demonstrate reversible hydrogenation by replacing MMA with dielectrics such as SiO_2 . We show the reversible hydrogenation, however, by measuring the resistance of graphene, which indicates its transition from semimetal to insulator upon hydrogenation and back to a semimetal upon annealing (Supporting Information Figure S14).

In summary, we developed a formalism for the generalized Brewster effect in the context of thin-film light absorbers. The experimental demonstrations confirm the existence of a Brewster angle for both s- and p-polarized light where the light is polarized by reflection due to polarization-dependent perfect light absorption. Furthermore, by using an ultrathin lossless dielectric film on a lossy substrate, we realized the s-polarized Brewster effect using a thin-film-based metasurface, which can act as an effective medium with a tunable Brewster angle. With the high phase sensitivity near the GBA, it is possible to monitor slight changes in the electromagnetic environment of the thin-film device, which enables a lithography-free ultrasensitive platform. In particular, we showed a hydrogen sensor with readily available and cheap materials, namely, Si, MMA, and graphene, without any nanofabrication and without the need to couple graphene to a surface plasmon based sensor to indirectly probe the changes in graphene or other 2D materials' optical properties.⁵⁰ The device can also function as a platform for other graphene-based sensors, in particular, for the development of cost-effective apta-biosensor platforms.⁵¹ The effect can be used to realize polarizers for both s- and p-polarizations, as well as for ultrafast polarization switches.⁵² Furthermore, it can be used for the Brewster window in gas lasers and the optical broadband angular selectivity¹⁴ as well as for Brewster angle microscopy.³

■ ASSOCIATED CONTENT

Supporting Information

The Supporting Information is available free of charge on the ACS Publications website at DOI: 10.1021/acsp Photonics.9b00564.

Sample fabrication and characterizations; angular reflection measurements; spectroscopic ellipsometry characterizations; hydrogenation of graphene-based thin-film absorbers; and additional experimental and simulation results (PDF)

■ AUTHOR INFORMATION

Corresponding Authors

*E-mail: guo@optics.rochester.edu (C. Guo).

*E-mail: ranjans@ntu.edu.sg (R. Singh).

ORCID

Chunlei Guo: 0000-0001-8525-6301

Ranjan Singh: 0000-0001-8068-7428

Author Contributions

□K.V.S. and M.E. contributed equally to this work.

Notes

The authors declare no competing financial interest.

■ ACKNOWLEDGMENTS

The authors acknowledge the financial support from the Ministry of Education AcRF Tier 1 grant RG191/17 and Tier 2 grant MOE2015-T2-2-103. We also acknowledge the financial support from Bill & Melinda Gates Foundation OPP1119542 and the U.S. Army Research Office (ARO).

■ REFERENCES

- (1) Brewster, D. On the laws which regulate the polarisation of light by reflexion from transparent bodies. *Philos. Trans. R. Soc. London* **1815**, *105*, 125–159.
- (2) Chen, Z.; Chen, X.; Tao, L.; Chen, K.; Long, M.; Liu, X.; Yan, K.; Stantchev, R. I.; Pickwell-MacPherson, E.; Xu, J.-B. Graphene controlled Brewster angle device for ultra-broadband terahertz modulation. *Nat. Commun.* **2018**, *9*, 4909.
- (3) Hoenig, D.; Moebius, D. Direct visualization of monolayers at the air–water interface by Brewster angle microscopy. *J. Phys. Chem.* **1991**, *95*, 4590–4592.
- (4) Kravets, V. G.; Schedin, F.; Jalil, R.; Britnell, L.; Gorbachev, R. V.; Ansell, D.; Thackray, B.; Novoselov, K. S.; Geim, A. K.; Kabashin, A. V.; Grigorenko, A. N. Singular phase nano-optics in plasmonic metamaterials for label-free single-molecule detection. *Nat. Mater.* **2013**, *12*, 304–309.
- (5) Giles, C. L.; Wild, W. J. Brewster angles for magnetic media. *Int. J. Infrared Millimeter Waves* **1985**, *6*, 187–197.
- (6) Heading, J. Generalized Investigations into the Brewster Angle. *Opt. Acta* **1986**, *33*, 755–770.
- (7) Shalaev, V. M. Optical negative-index metamaterials. *Nat. Photonics* **2007**, *1*, 41–48.
- (8) Zheludev, N. I. The road ahead for metamaterials. *Science* **2010**, *328*, 582–583.
- (9) Fu, C.; Zhang, Z. M.; First, P. N. Brewster angle with a negative-index material. *Appl. Opt.* **2005**, *44*, 3716–3724.
- (10) Tamayama, Y.; Nakanishi, T.; Sugiyama, K.; Kitano, M. Observation of Brewster's effect for transverse-electric electromagnetic waves in metamaterials: Experiment and theory. *Phys. Rev. B: Condens. Matter Mater. Phys.* **2006**, *73*, 193104.
- (11) Tamayama, Y. Brewster effect in metafilms composed of bi-anisotropic split-ring resonators. *Opt. Lett.* **2015**, *40*, 1382–1385.
- (12) Paniagua-Domínguez, R.; Yu, Y. F.; Miroshnichenko, A. E.; Krivitsky, L. A.; Fu, Y. H.; Valuckas, V.; Gonzaga, L.; Toh, Y. T.; Kay, J. C. *Nat. Commun.* **2015**, *6*, 7442.

A. Y. S.; Luk'yanchuk, B.; Kuznetsov, A. I. Generalized Brewster effect in dielectric metasurfaces. *Nat. Commun.* **2016**, *7*, 10362.

(13) Watanabe, R.; Iwanaga, M.; Ishihara, T. s-polarization Brewster's angle of stratified metal-dielectric metamaterial in optical regime. *Phys. Status Solidi B* **2008**, *245*, 2696–2701.

(14) Lin, X.; Shen, Y.; Kammer, I.; Chen, H.; Soljačić, M. Transverse-electric Brewster effect enabled by nonmagnetic two-dimensional materials. *Phys. Rev. A: At., Mol., Opt. Phys.* **2016**, *94*, 023836.

(15) Lakhtakia, A. Would Brewster recognize today's Brewster angle. *Optics News* **1989**, *15*, 14–18.

(16) Bassiri, S.; Papas, C. H.; Engheta, N. Electromagnetic wave propagation through a dielectric-chiral interface and through a chiral slab. *J. Opt. Soc. Am. A* **1988**, *5*, 1450–1459.

(17) Mahlein, H. F. Generalized Brewster-angle conditions for quarter-wave multilayers at non-normal incidence. *J. Opt. Soc. Am.* **1974**, *64*, 647–653.

(18) Sotiropoulos, D. A.; Ogden, R. W. Generalized Brewster angle for wave reflection from a fluid-transversely isotropic solid interface. *Ultrasonics* **1996**, *34*, 487–489.

(19) Ruiz-Urbieta, M.; Sparrow, E. M. Reflection polarization by a transparent-film-absorbing-substrate system. *J. Opt. Soc. Am.* **1972**, *62*, 1188–1194.

(20) Azzam, R. M. A. Single-layer antireflection coatings on absorbing substrates for the parallel and perpendicular polarizations at oblique incidence. *Appl. Opt.* **1985**, *24*, 513–518.

(21) Azzam, R. M. A.; Thonn, T. F. Pseudo-Brewster and second-Brewster angles of an absorbing substrate coated by a transparent thin film. *Appl. Opt.* **1983**, *22*, 4155–4166.

(22) Kitajima, H.; Fujita, K.; Cizmic, H. Zero reflection from a dielectric film on metal substrate at oblique angles of incidence. *Appl. Opt.* **1984**, *23*, 1937–1939.

(23) Azzam, R. M. A. Extinction of the p and s polarizations of a wave on reflection at the same angle from a transparent film on an absorbing substrate: applications to parallel-mirror crossed polarizers and a novel integrated polarimeter. *J. Opt. Soc. Am. A* **1985**, *2*, 189–197.

(24) Azzam, R. M. A. Explicit equations for the polarizing angles of a high-reflectance substrate coated by a transparent thin film. *J. Opt. Soc. Am. A* **1985**, *2*, 480–482.

(25) Chilwell, J.; Hodgkinson, I. Thin films field-transfer matrix theory of planar multilayer waveguides and reflection from prism-loaded waveguides. *J. Opt. Soc. Am. A* **1984**, *1*, 742.

(26) Sreekanth, K. V.; Sreejith, S.; Han, S.; Mishra, A.; Chen, X.; Sun, H.; Lim, C.-T.; Singh, R. Biosensing with the singular phase of an ultrathin metal-dielectric nanophotonic cavity. *Nat. Commun.* **2018**, *8*, 369.

(27) Sreekanth, K. V.; Han, S.; Singh, R. Ge₂Sb₂Te₅-based tunable perfect absorber cavity with phase singularity at visible frequencies. *Adv. Mater.* **2018**, *30*, 706696.

(28) ElKabbash, M.; Iram, S.; Letsou, T.; Hinczewski, M.; Strangi, G. Designer perfect light absorption using ultrathin lossless dielectrics on absorptive substrates. *Adv. Opt. Mater.* **2018**, *6*, 1800672.

(29) Kats, M. A.; Blanchard, R.; Genevet, P.; Capasso, F. Nanometre optical coatings based on strong interference effects in highly absorbing media. *Nat. Mater.* **2013**, *12*, 20–24.

(30) Yu, N.; Capasso, F. Flat optics with designer metasurfaces. *Nat. Mater.* **2014**, *13*, 139–150.

(31) Gu, H.; Wang, Z.; Hu, Y. Hydrogen gas sensors based on semiconductor oxide nanostructures. *Sensors* **2012**, *12*, 5517–5550.

(32) Wadell, C.; Syrenova, S.; Langhammer, C. Plasmonic hydrogen sensing with nanostructured metal hydrides. *ACS Nano* **2014**, *8*, 11925–11940.

(33) Wilkins, J. R.; Stoner, G. E.; Boykin, E. H. Microbial detection method based on sensing molecular-hydrogen. *Appl. Microbiol.* **1974**, *27*, 949–952.

(34) Hitchcock, C. H. S. Determination of hydrogen as a marker in irradiated frozen food. *J. Sci. Food Agric.* **2000**, *80*, 131–136.

(35) Tittel, A.; Kremers, C.; Dorfmüller, J.; Chigrin, D. N.; Giessen, H. Spectral shifts in optical nanoantenna-enhanced hydrogen sensors. *Opt. Mater. Express* **2012**, *2*, 111–118.

(36) Nasir, M. E.; Dickson, W.; Wurtz, G. A.; Wardley, W. P.; Zayats, A. V. Hydrogen detected by the naked eye: optical hydrogen gas sensors based on core/shell plasmonic nanorod metamaterials. *Adv. Mater.* **2014**, *26*, 3532–3537.

(37) Tittel, A.; Mai, P.; Taubert, R.; Dregely, D.; Liu, N.; Giessen, H. Palladium-based plasmonic perfect absorber in the visible wavelength range and its application to hydrogen sensing. *Nano Lett.* **2011**, *11*, 4366.

(38) Chadwick, B.; Gal, M. Enhanced optical detection of hydrogen using the excitation of surface plasmons in palladium. *Appl. Surf. Sci.* **1993**, *68*, 135–138.

(39) Maeda, E.; Mikuriya, S.; Endo, K.; Yamada, I.; Suda, A.; Delaunay, J.-J. Optical hydrogen detection with periodic subwavelength palladium hole arrays. *Appl. Phys. Lett.* **2009**, *95*, 133504.

(40) Perrotton, C.; Westerwaal, R. J.; Javahiry, N.; Slaman, M.; Schreuders, H.; Dam, B.; Meyrueis, P. A reliable, sensitive and fast optical fiber hydrogen sensor based on surface plasmon resonance. *Opt. Express* **2013**, *21*, 382–390.

(41) Langhammer, C.; Zoric, I.; Kasemo, B. Hydrogen storage in Pd nanodisks characterized with a novel nanoplasmonic sensing scheme. *Nano Lett.* **2007**, *7*, 3122–3127.

(42) Shegai, T.; Johansson, P.; Langhammer, C.; Kall, M. Directional scattering and hydrogen sensing by bimetallic Pd-Au nanoantennas. *Nano Lett.* **2012**, *12*, 2464–2469.

(43) Elias, D. C.; Nair, R. R.; Mohiuddin, T. M. G.; Morozov, S. V.; Blake, P.; Halsall, M. P.; Ferrari, A. C.; Boukhvalov, D. W.; Katsnelson, M. I.; Geim, A. K.; Novoselov, K. S. Control of graphene properties by reversible hydrogenation: Evidence for graphane. *Science* **2009**, *323*, 610–613.

(44) Kravets, V. G.; Schedin, F.; Jalil, R.; Britnell, L.; Novoselov, K. S.; Grigorenko, A. N. J. Surface hydrogenation and optics of a graphene sheet transferred onto a plasmonic nanoarray. *J. Phys. Chem. C* **2012**, *116*, 3882–3887.

(45) Song, H.; Guo, L.; Liu, Z.; Liu, K.; Zeng, X.; Ji, D.; Zhang, N.; Hu, H.; Jiang, S.; Gan, Q. Nanocavity enhancement for ultra-thin film optical absorber. *Adv. Mater.* **2014**, *26*, 2737–2743.

(46) Bruna, M.; Borini, S. Optical constants of graphene layers in the visible range. *Appl. Phys. Lett.* **2009**, *94*, 031901.

(47) Zhu, J.; Yan, S.; Feng, N.; Ye, L.; Ou, J.-Y.; Liu, Q. H. Near unity ultraviolet absorption in graphene without patterning. *Appl. Phys. Lett.* **2018**, *112*, 153106.

(48) Lin, H.; Sturmberg, B. C. P.; Lin, K.-T.; Yang, Y.; Zheng, X.; Chong, T. K.; de Sterke, C. M.; Jia, B. A 90-nm-thick graphene metamaterial for strong and extremely broadband absorption of unpolarized light. *Nat. Photonics* **2019**, *13*, 270–276.

(49) Lee, C.; Leconte, N.; Kim, J.; Cho, D.; Lyo, I.-W.; Choi, E. J. Optical spectroscopy study on the effect of hydrogen adsorption on graphene. *Carbon* **2016**, *103*, 109–114.

(50) Donarelli, M.; Ottaviano, L. 2D materials for gas sensing applications: A review on graphene oxide, MoS₂, WS₂ and Phosphorene. *Sensors* **2018**, *18*, 3638.

(51) Justino, C. I. L.; Gomes, A. R.; Freitas, A. C.; Duarte, A. C.; Rocha-Santos, A. P. Graphene based sensors and biosensors. *TrAC, Trends Anal. Chem.* **2017**, *91*, 53–66.

(52) Yang, Y.; Kelley, K.; Sachet, E.; Campione, S.; Luk, S. T.; Maria, J.-P.; Sinclair, M. B.; Berner, I. Femtosecond optical polarization switching using a cadmium oxide-based perfect absorber. *Nat. Photonics* **2017**, *11*, 390–395.